Physics of the Earth and Planetary Interiors, 75 (1993) 243–266
Elsevier Science Publishers B.V., Amsterdam

Significance of non-double couple components of deep and intermediate-depth earthquakes: implications from moment tensor inversions of long-period seismic waves

Keiko Kuge [a] and Hitoshi Kawakatsu [b]

[a] *Department of Geophysics, Faculty of Science, Kyoto University, Kyoto 606-01, Japan*
[b] *Geological Survey of Japan, Tsukuba 305, Japan*

(Received 27 April 1992; accepted 7 July 1992)

ABSTRACT

Kuge, K. and Kawakatsu, H., 1993. Significance of non-double couple components of deep and intermediate-depth earthquakes: implications from moment tensor inversions of long-period seismic waves. Phys. Earth Planet. Inter., 75: 243–266.

Analysis of long-period seismic waves suggests that non-double couple components in source moment tensors of intermediate-depth and deep earthquakes are significant and appear to respond to the state of predominant strain release within slabs. The strain regime is partially or fully induced by the sources themselves or by slab structures near the sources. We observe consistency in the non-double couple components from three different seismic wave inversions. Among 21 earthquakes studied, 17 events have the same sign in the three non-double couple components, and the signs show a correlation with the state of strain release within the slabs. The effects of unmodeled propagation structure and instability of the inversion procedure are unlikely to be responsible for the consistent non-double couple components because the suites of seismic waves traverse different paths and the various inversion schemes have the different resolvabilities of the moment tensors.

1. Introduction

It has been observed that some earthquakes have moment tensors with a significant departure from a purely double couple source, that is, earthquakes may have 'non-double couple components'. Examples include the May 1980 Mammoth Lakes shallow earthquakes (Barker and Langston, 1983; Ekström and Dziewonski, 1985), the 26 January 1983 Kermadec intermediate-depth earthquake (Riedesel and Jordan, 1989), and the 1 January 1984 South of Honshu, Japan, deep earthquake (Ekström et al., 1986). In waveform analyses, moment tensors are estimated after deconvolving the responses of the Earth from the observed seismograms. As most earthquakes are well represented by double couple focal mechanisms, it is often suspected that the non-double couple components are caused by the inversion procedure (for example, problems with the observed data, such as low signal-to-noise ratio, or errors in the assumed responses of the Earth). Doornbos (1985) suggested that using different velocity structures and station time corrections can cause significant fluctuation of the non-double couple components. Solomon and Julian (1974) proposed that effects of heterogeneous structure along the ray paths may explain non-double couple earthquakes. Lack of appropriate station coverage can also produce apparent non-double couple components (Satake, 1985).

On the other hand, Giardini (1983, 1984) detected a relationship between non-double couple

Correspondence to: K. Kuge, Institute of Tectonics, University of California, Santa Cruz, CA 95064, USA.

0031-9201/93/$06.00 © 1993 – Elsevier Science Publishers B.V. All rights reserved

components of intermediate-depth and deep earthquakes and the predominant strain release within subducting slabs. For shallow earthquakes, Kawakatsu (1991b) pointed out that the geographical distribution of non-double couple components has a clear correlation with the plate tectonic environment. The non-double couple components may thus be more than simply reflections of errors in the data and inversion procedures and may reveal important source physics.

As the physical mechanisms responsible for intermediate-depth and deep earthquakes are not yet understood, explaining the origins of non-double couple components of intermediate-depth and deep events is especially important. Experimental studies under non-hydrostatic pressure show that a shear dislocation nucleates from the $\alpha \rightarrow \gamma$ phase transformation of Mg_2GeO_4 under metastable conditions (Green and Burnley, 1989; Burnley et al., 1991) as well as the $\alpha \rightarrow \beta$ transformation of metastable natural olivine (Green et al., 1990). Green and Burnley (1989) proposed that an analogous process can produce deep earthquakes (depth greater than 300 km). Moment tensors excited by these sources, however, are expected to correspond to basically double couple mechanisms. If a significant non-double couple component in the moment tensor is intrinsic for deep earthquakes, some other physical mechanisms may be necessary to explain the source process.

In this study, we evaluate the significance of previously reported non-double couple components of 21 large intermediate-depth and deep earthquakes by using several different phases on long-period waveforms. We also examine the statistical nature of non-double couple components of the Harvard centroid-moment tensor (CMT) solutions in relation to the states of strain release within slabs. As the isotropic non-double couple component is difficult to constrain (e.g. Kawakatsu, 1991a, 1992), we deal with only the deviatoric non-double couple component here. This is defined, following Giardini (1983, 1984), by

$$\epsilon = -\frac{\lambda_2}{\max(|\lambda_1|, |\lambda_3|)} \qquad (1)$$

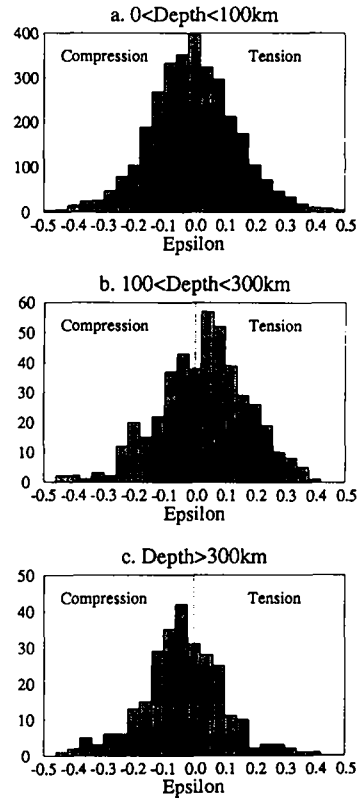

Fig. 1. Histograms of non-double couple components (ϵ) of the Harvard centroid-moment tensor (CMT) solutions during the period between 1977 and January 1991 (log M_0[N m] $\geq$ 17.5). (a) Shallow earthquakes (depth less than 100 km); (b) intermediate-depth earthquakes (100 km $\leq$ depth $<$ 300 km); (c) deep earthquakes (depth 300 km or greater).

where λ_i represents an eigenvalue of moment tensor ($\lambda_1 \geq \lambda_2 \geq \lambda_3$). The parameter ϵ is zero in the case of a double couple source, and ± 0.5 in the case of compensated linear vector dipole (CLVD; Knopoff and Randall, 1970) sources.

2. Non-double couple components and strain release within subducting slabs

Figure 1 shows histograms of non-double couple components of the Harvard CMT solutions for three depth ranges. Dotted lines indicate ϵ = 0, which corresponds to purely double couple mechanisms. We observe different distributions of ϵ for shallow, intermediate-depth and deep

events. For shallow events, ϵ distributes more or less evenly around zero. The distribution of ϵ for intermediate-depth earthquakes is shifted slightly toward positive values, whereas the distribution of ϵ for deep events is shifted toward negative values. The average ϵ values are 0.00 ± 0.14 (shallow events), 0.03 ± 0.15 (intermediate-depth events), and -0.04 ± 0.14 (deep events). Positive ϵ means that the maximum absolute eigenvalue is the tensional principal axis (T-axis), that is, predominantly tensional strain. Negative ϵ means that the maximum absolute eigenvalue is the compressional principal axis (P-axis), that is, predominantly compressional strain. Focal mechanisms of intermediate-depth and deep earthquakes are generally characterized respectively by predominantly tensional and compressional strain state within slabs (Isacks and Molnar, 1969). Figure 1 thus shows that ϵ of intermediate-depth and deep earthquakes may reflect the general strain release environment within the slabs.

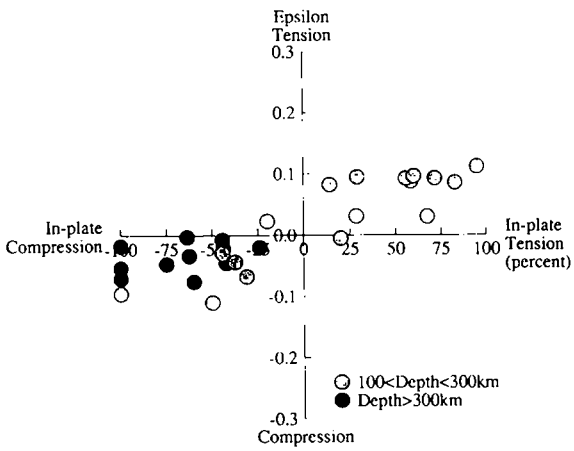

Fig. 2. States of strain release and average non-double couple components (ϵ) of 17 subducting slabs. The average ϵ of events within a slab is represented on the vertical axis. We define an 'in-plate' stress event as an event for which the principal axes are in the range of planes that are parallel to the slab and within 25° of the dip angle of the slab on the unit focal sphere. We obtain the ratio of in-plate tensional events (γ_T) and the ratio of in-plate compressional events (γ_P); $\gamma_T = N_T/N$ and $\gamma_P = N_P/N$, where N_T, N_P, and N are the number of in-plate tensional events, the number of compressional events, and the total number of events, respectively. We use the Harvard CMT solutions (1977–January, 1991; $\log M_0$[N m] ≥ 17.5). The horizontal axis shows the difference $[(\gamma_T - \gamma_P) \times 100(\%)]$ between the two ratios in each region. For the dipping and strike angles of the slabs, we use the data of Kawakatsu (1986), except for South America and Philippine, for which we determine the angles from recent hypocentral distribution in the International Seismological Center (ISC) bulletin. The studied regions, the average ϵ, and the ratios are shown in Table 1.

Even on a regional scale, we observe a similar relationship between ϵ and the state of strain release within the slab. Figure 2 shows a correlation between the strain release within the subducting slab and the average ϵ in 17 subducting regions. We define 'in-plate stress' events for which the principal axes are in the range of planes that are parallel to the slab and within 25° of the dip angle of the slab on the unit focal sphere, which is similar to the definition of Fujita and Kanamori (1981). We compute the ratio of in-plate tensional events (γ_T) and the ratio of in-plate compressional events (γ_P); $\gamma_T = N_T/N$, and $\gamma_P = N_P/N$, where N_T, N_P, and N are the number of in-plate tensional events, the number of in-plate compressional events, and the total number of events in each slab, respectively. The studied regions and the ratios are shown in Table 1. The horizontal axis of Fig. 2 indicates the difference $((\gamma_T - \gamma_P) \times 100(\%))$ between the two ratios in each region. The vertical axis represents the average ϵ ($\bar{\epsilon}$) in each subduction zone. Positive $\bar{\epsilon}$ tends to be observed in slabs with predominantly tensional strain release, whereas slabs with predominantly compressional strain release are accompanied by negative $\bar{\epsilon}$. There appears to be a correlation between the strain release within the slab and $\bar{\epsilon}$.

3. Non-double couple components observed in three different inversion schemes

For 21 earthquakes with large non-double couple components reported in the Harvard CMT solutions, we examine the significance of the non-double couple components using three different moment tensor inversions of long-period seismic waves. Table 2 lists the deep ($\text{depth}_{PDE} \geq 300$ km and $M_0 > 10^{18}$ N m) and intermediate-depth (100 km $\leq \text{depth}_{PDE} < 300$ km and $M_0 > 5 \times 10^{18}$ N m) earthquakes during the period

TABLE 1

Strain release within slabs and ϵ in 17 subduction zones

	Pole		Lat. (deg)		Long. (deg)		Dip angle (deg)	Number	100 km ≤ depth < 300 km		ϵ	Number	Depth ≥ 300 km		ϵ
	Lat. (deg)	Long. (deg)							In-plate P(%)	In-plate T(%)			In-plate P(%)	In-plate T(%)	
Aleutians	65.0	180.4	45.0	62.0	165.0	−155.0	55.0	5	60.0	40.0	0.02	–	–	–	–
Bonin	6.4	75.1	25.0	35.0	135.0	145.0	55.0	7	100.0	0.0	−0.10	25	68.0	24.0	−0.02
Mid-America	29.4	282.3	5.0	20.0	−100.0	−80.0	50.0	12	16.7	75.0	0.09	–	–	–	–
Japan	37.9	113.1	35.0	45.0	130.0	145.0	30.0	7	14.3	28.6	0.08	11	81.8	18.2	−0.00
Java	39.2	120.8	−12.0	−3.0	100.0	135.0	60.0	31	38.7	67.7	0.09	29	44.8	20.7	−0.02
Kurile	57.8	128.9	43.0	60.0	142.0	170.0	45.0	16	68.8	37.5	−0.07	12	83.3	8.3	−0.05
Tonga	22.4	80.1	−27.0	−13.0	174.0	−168.0	55.0	63	69.8	25.4	−0.03	144	76.4	34.0	−0.05
Kermadec	−22.4	159.9	−36.0	−27.0	174.0	−168.0	62.0	8	75.0	37.5	−0.04	5	80.0	20.0	−0.08
Mariana	17.3	139.1	10.0	26.0	135.0	150.0	70.0	15	40.0	60.0	−0.01	8	75.0	12.5	−0.03
Vanuatu	−1.7	−157.9	−25.0	−10.0	164.0	175.0	70.0	55	20.0	87.3	0.03	–	–	–	–
N. Ryukyu	35.5	116.3	28.0	35.0	127.0	133.0	70.0	7	14.3	85.7	0.09	–	–	–	–
S. Ryukyu	35.5	116.3	24.0	28.0	120.0	128.0	45.0	4	75.0	25.0	−0.11	–	–	–	–
Scotia	−58.0	−31.8	−64.0	−52.0	−40.0	−15.0	50.0	9	22.2	77.8	0.09	–	–	–	–
	Strike N(deg)E		Lat. (deg)		Long. (deg)		Dip angle (deg)	Number	100 km ≤ depth < 300 km		ϵ	Number	Depth ≥ 300 km		ϵ
									In-plate P(%)	In-plate T(%)			In-plate P(%)	In-plate T(%)	
Peru	−10.0		−14.0	−7.0	−84.0	−58.0	7.0 (85)	5	0.0	60.0	0.10	8	100.0	0.0	−0.02
Antiplano	−30.0		−20.1	−14.0	−84.0	−58.0	30.0	23	0.0	82.6	0.09	1	100.0	0.0	−0.05
Chile	0.0		−33.6	−20.1	−84.0	−58.0	30.0	40	0.0	95.0	0.11	9	55.6	11.1	−0.01
Philippine	−165.0		−3.0	7.0	120.0	127.0	60.0	21	33.3	61.9	0.03	8	100.0	0.0	−0.07

The dip angle for the deep slab is shown in parentheses.

1977–1987 which have large $|\epsilon|$ (greater than 0.15) in the Harvard CMT solutions. The locations are shown in Fig. 3. We exclude earthquakes for which few direct P and SH waves were recorded (e.g. events beneath South America). The moment tensors are estimated by modeling three different sets of seismic waves with different frequency bands: centroid moment tensor (CMT) inversion of surface waves (3.5–10 mHz), CMT inversion of long-period body wavetrains (12–20 mHz), and a waveform inversion of isolated P and SH body waves from the Global Digital Seismographic Network (GDSN) long-period channels (GDSN LP inversions) (approximately 40 mHz). The moment tensor solutions are summarized in Table 3.

3.1. CMT inversions

Moment tensor representations are retrieved from surface waves and long-period body waves separately using the CMT inversion program coded by Kawakatsu (1989). The inversion method follows Dziewonski et al. (1981) and Dziewonski and Woodhouse (1983a, b). For computing normal modes, we use Earth model 1066a (Gilbert and Dziewonski, 1975) and the Q^{-1} model of Masters and Gilbert (1983). Data are from long-period channels of GDSN stations. For surface waves, we also use very-long-period channels of International Deployment of Accelerometers (IDA) and GEOSCOPE stations. Surface waves are bandpass filtered between 3.5 and 10.0 mHz. We adjust the passband to the magnitude of the earthquake, shifting it slightly to high frequencies when the event is small, and to low frequencies when the event is large. Surface wavetrains along the minor arc are modeled for all events except for the 24 November 1983 Banda Sea earthquake. As the minor arc surface waves from the Banda Sea event are mostly off scale, we use the major arc surface wavetrains. For the long-period body waves, we use the wavetrains from the P arrivals

TABLE 2

Deep and intermediate-depth earthquakes studied in this paper

Year	Month	Day	Lat. (°N)	Long. (°E)	Depth (km)	NDC?
Deep earthquakes						
1987	5	7	46.75	139.22	417.0	○
1986	6	16	−21.93	−178.96	557.0	○
1984	1	1	33.62	136.80	386.0	○
1984	3	5	8.17	123.77	656.0	○
1982	1	4	18.00	145.67	607.0	○
1982	7	4	27.90	137.04	554.0	○
1981	9	28	−29.41	−179.03	274.0	○
1981	10	7	−20.70	−178.65	606.0	○
1980	3	31	35.49	135.52	362.0	×
1978	3	7	31.99	137.61	441.0	×
Intermediate-depth earthquakes						
1986	5	11	26.73	125.26	200.0	○
1985	4	23	15.32	120.63	181.0	○
1985	10	9	−6.76	107.04	104.0	○
1984	10	15	−15.75	−173.65	80.0	○
1983	1	26	−30.44	−179.30	208.0	○
1983	8	25	33.51	131.51	128.0	○
1983	11	24	−7.47	128.20	183.0	○
1982	9	6	29.40	140.43	179.0	○
1980	7	8	6.63	125.77	185.0	×
1979	8	5	−22.86	−177.47	204.0	×
1978	3	15	26.45	140.76	278.0	○

ISC hypocenters are shown. For earthquakes with circles in the column 'NDC?', we observe consistent signs of the non-double couple components (ϵ) obtained from three different inversions (see Table 3), whereas we do not for earthquakes with crosses.

to just before the Love wave arrivals, bandpass filtered between 12 and 20 mHz.

3.2. *GDSN LP inversions*

We invert GDSN long-period P and SH waveforms using a scheme based on ray theory. The peak frequency of the instrumental response for GDSN long-period seismograms is around 40 mHz. The inversion scheme closely follows that of Nábělek (1984). A source time function and a moment tensor are simultaneously estimated in the inversion. The source time function is described as a sum of symmetric triangles whose half-duration is 2 s. Geometrical spreading factors and ray parameters are computed from the isotropic Preliminary Reference Earth Model (PREM) (1 Hz) (Dziewonski and Anderson, 1981). We align the seismograms by maximizing the correlation coefficient between synthetic and observed waveforms. We use the inverse of the power of each observed seismogram as a weighting factor, to give equal weight to all the seismograms.

For deep earthquakes, pP waves are well separated from P and sP waves, and we separately model P, pP, and SH waves. For intermediate-depth events, the depth phases (pP and sP) arrive just after the P wave. As well as the direct SH waves, we model P wavetrains of 100–120 s length of P, pP, and sP waves instead of separately modeling the P and pP waves. Waveforms of the P wavetrains strongly depend on the source depth through the arrival times of pP and sP waves. After performing several inversions at various source depths, we choose a moment tensor solution at the depth which maximizes the variance reduction.

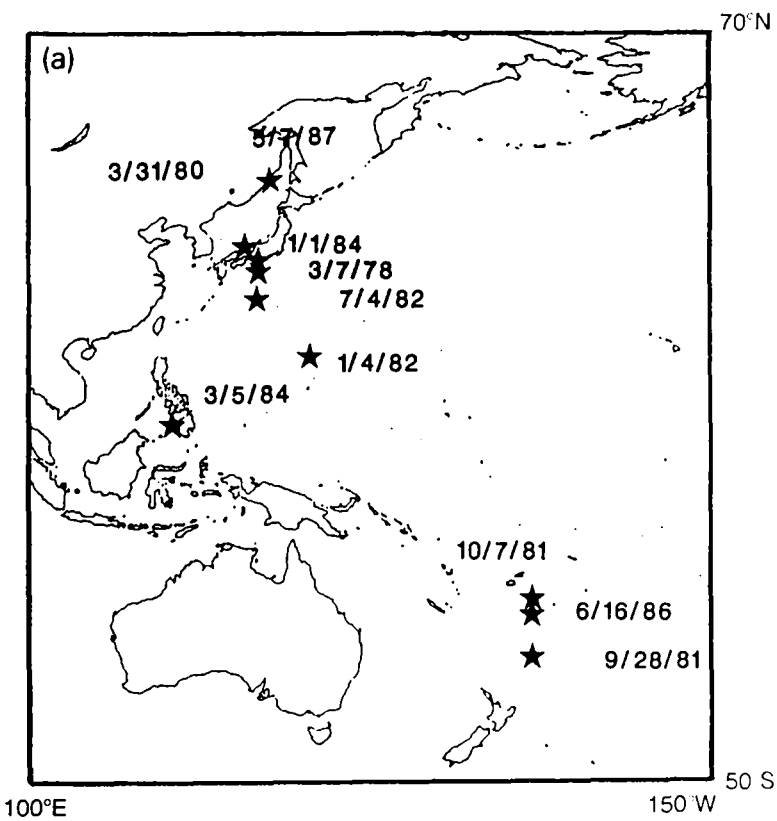

Fig. 3. Epicenters of the studied non-double couple earthquakes. (a) Deep earthquakes (depth 300 km or greater); (b) intermediate-depth earthquakes (100 km ≤ depth < 300 km).

3.3. *Error estimates of non-double couple components*

As ϵ is not a linear parameter of a moment tensor, the error estimate of ϵ is rather complicated. By means of a non-linear minimization technique (Gill et al., 1981), Vasco (1990) suggested estimating the extremal values of a non-double couple component by assuming some error ranges on the observed waveforms. As we model thousands of waveform data points in the time domain in CMT inversions, it is difficult to use the extremal approach directly. Using the covariance matrix for the moment tensor, we instead attempt a simple perturbation approach to check the stability of ϵ. For the covariance matrix, we use a degree of freedom in the frequency domain instead of a degree of freedom in the time domain (i.e. the number of data points) because the real degree of freedom of the data should be less than the number of the data points when the data are bandpass-filtered.

A covariance matrix for the eigenvalues of the moment tensor is obtained from a linear transformation of the covariance matrix of moment tensor components (e.g. Riedesel and Jordan, 1989). For small perturbations of the eigenvalues, the ϵ range is approximated to the first order as follows:

$$\epsilon \pm \Delta\epsilon \approx -\frac{\lambda_2 \pm \delta\lambda_2}{|\lambda_j \pm \delta\lambda_j|}$$

$$\approx -\frac{\lambda_2}{|\lambda_j|}\left(1 \pm \frac{\delta\lambda_2}{|\lambda_2|} \pm \frac{\delta\lambda_j}{|\lambda_j|}\right) \qquad (2)$$

$j = 1$ if $|\lambda_1| > |\lambda_3|$

$j = 3$ if $|\lambda_1| < |\lambda_3|$

where λ_j is the eigenvalue of the moment tensor ($\lambda_1 > \lambda_2 > \lambda_3$). Using the standard errors of eigenvalues (σ_λ) for $\delta\lambda_j$, we obtain the ϵ range shown in Table 3.

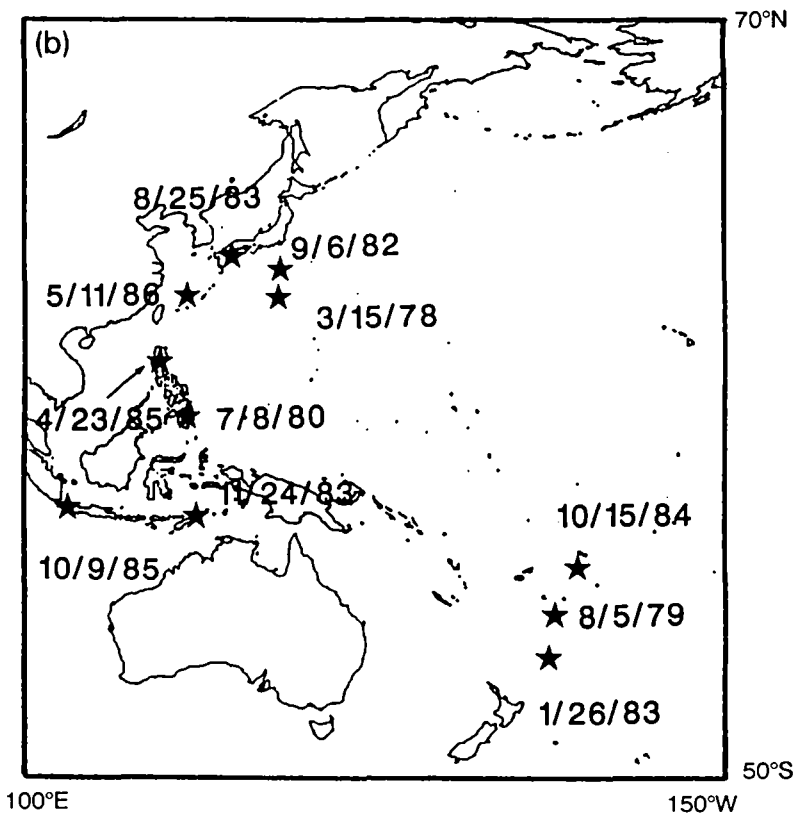

Fig. 3 (continued).

3.4. *Effect of non-linear parameters*

Estimation of the source location has non-linear effects on the moment tensor inversion. Both the centroid location and moment tensor are determined in a CMT inversion. For GDSN LP inversions for intermediate-depth events, source depth is determined from several inversions at

TABLE 3(a)

Moment tensor solutions from three moment tensor inversions for deep earthquakes

	CMT surface	CMT body	GDSN LP		CMT surface	CMT body	GDSN LP
7 May 1987. N. Sea of Japan, 417 km, $\epsilon = -0.22 \pm 0.03$				*4 January 1982. Mariana, 607 km, $\epsilon = -0.22 \pm 0.09$*			
M_0	1.720	1.372	1.773	M_0	0.657	0.544	0.966
M_{xx}	0.619 ± 0.031	0.459 ± 0.028	0.693 ± 0.058	M_{xx}	0.167 ± 0.015	0.135 ± 0.019	0.409 ± 0.098
M_{yy}	-1.418 ± 0.047	-1.029 ± 0.044	-1.465 ± 0.060	M_{yy}	0.472 ± 0.021	0.419 ± 0.025	0.629 ± 0.085
M_{zz}	0.800 ± 0.023	0.569 ± 0.023	0.772 ± 0.059	M_{zz}	-0.639 ± 0.017	-0.553 ± 0.025	-1.038 ± 0.117
M_{xy}	0.847 ± 0.035	0.618 ± 0.033	0.976 ± 0.062	M_{xy}	0.145 ± 0.016	0.082 ± 0.023	0.114 ± 0.075
M_{xz}	0.276 ± 0.014	0.209 ± 0.027	0.221 ± 0.032	M_{xz}	-0.086 ± 0.014	-0.033 ± 0.022	-0.013 ± 0.046
M_{yz}	0.886 ± 0.029	0.853 ± 0.038	0.855 ± 0.036	M_{yz}	$-0.289 + 0.018$	-0.218 ± 0.022	-0.454 ± 0.072
ϵ	-0.22 ± 0.02	-0.20 ± 0.03	-0.25 ± 0.03	ϵ	-0.15 ± 0.03	-0.19 ± 0.04	-0.32 ± 0.11
η_P	0.992	1.000	0.983	η_P	0.993	1.000	0.986
η_H	0.991	1.000	0.981	η_H	0.984	1.000	0.941
16 June 1986. Tonga, 557 km, $\epsilon = -0.15 \pm 0.04$				*4 July 1982. Bonin, 554 km, $\epsilon = 0.15 \pm 0.04$*			
M_0	4.416	3.623	5.335	M_0	0.894	0.982	1.434
M_{xx}	2.164 ± 0.103	1.660 ± 0.085	2.814 ± 0.475	M_{xx}	0.477 ± 0.030	0.343 ± 0.024	1.525 ± 0.149
M_{yy}	1.280 ± 0.097	0.639 ± 0.090	2.144 ± 0.478	M_{yy}	-0.232 ± 0.022	-0.152 ± 0.024	-0.179 ± 0.101
M_{zz}	-3.443 ± 0.089	-2.298 ± 0.074	-4.958 ± 0.735	M_{zz}	-0.245 ± 0.019	-0.191 ± 0.015	-0.346 ± 0.089
M_{xy}	-1.239 ± 0.127	-0.585 ± 0.087	-1.361 ± 0.323	M_{xy}	0.318 ± 0.027	0.312 ± 0.026	0.534 ± 0.087
M_{xz}	-1.760 ± 0.088	-1.842 ± 0.083	-1.875 ± 0.212	M_{xz}	-0.743 ± 0.029	-0.888 ± 0.027	-1.262 ± 0.043
M_{yz}	2.449 ± 0.083	2.332 ± 0.079	2.345 ± 0.275	M_{yz}	0.057 ± 0.013	0.045 ± 0.019	$-0.012 + 0.077$
ϵ	-0.12 ± 0.03	-0.15 ± 0.02	-0.19 ± 0.11	ϵ	0.19 ± 0.03	0.12 ± 0.03	0.14 ± 0.05
η_P	0.975	1.000	0.929	η_P	0.984	1.000	0.996
η_H	0.980	1.000	0.972	η_H	0.986	1.000	0.997
1 January 1984. S. Honshu, 386 km, $\epsilon = -0.25 \pm 0.07$				*28 September 1981. Tonga, 274 km, $\epsilon = -0.18 \pm 0.15$*			
M_0	6.701	5.047	6.386	M_0	0.662	0.563	0.711
M_{xx}	2.602 ± 0.293	1.965 ± 0.119	1.941 ± 0.429	M_{xx}	-0.353 ± 0.022	-0.214 ± 0.024	0.140 ± 0.236
M_{yy}	-5.505 ± 0.455	-3.434 ± 0.188	-4.055 ± 0.359	M_{yy}	0.448 ± 0.020	0.358 ± 0.027	0.430 ± 0.096
M_{zz}	2.903 ± 0.207	1.469 ± 0.089	2.114 ± 0.210	M_{zz}	-0.095 ± 0.011	-0.144 ± 0.014	-0.570 ± 0.197
M_{xy}	-0.139 ± 0.352	0.137 ± 0.114	-0.039 ± 0.463	M_{xy}	-0.050 ± 0.015	-0.111 ± 0.019	-0.072 ± 0.122
M_{xz}	1.098 ± 0.093	0.808 ± 0.070	2.026 ± 0.138	M_{xz}	-0.459 ± 0.013	-0.392 ± 0.018	-0.536 ± 0.073
M_{yz}	5.001 ± 0.252	4.253 ± 0.141	5.050 ± 0.210	M_{yz}	0.256 ± 0.011	0.234 ± 0.018	0.134 ± 0.143
ϵ	$-0.30 + 0.05$	-0.29 ± 0.03	-0.18 ± 0.06	ϵ	-0.14 ± 0.02	-0.06 ± 0.04	-0.35 ± 0.25
η_P	0.985	1.000	0.984	η_P	0.983	1.000	0.825
η_H	0.992	1.000	0.984	η_H	0.988	1.000	0.919
5 March 1984. Mindanao, 656 km, $\epsilon = -0.28 \pm 0.10$				*7 October 1981. Tonga, 606 km, $\epsilon = -0.09 \pm 0.05$*			
M_0	9.639	8.077	7.027	M_0	0.670	0.570	0.928
M_{xx}	3.637 ± 0.146	3.299 ± 0.182	0.997 ± 0.958	M_{xx}	0.393 ± 0.020	0.356 ± 0.021	0.650 ± 0.058
M_{yy}	6.390 ± 0.181	5.281 ± 0.250	4.524 ± 1.227	M_{yy}	-0.012 ± 0.019	-0.005 ± 0.021	-0.015 ± 0.047
M_{zz}	-10.027 ± 0.199	-8.580 ± 0.286	-5.521 ± 1.280	M_{zz}	-0.381 ± 0.015	-0.351 ± 0.016	-0.635 ± 0.065
M_{xy}	-1.928 ± 0.219	-0.905 ± 0.231	-1.348 ± 0.695	M_{xy}	-0.101 ± 0.018	-0.087 ± 0.020	0.006 ± 0.076
M_{xz}	-4.025 ± 0.143	-4.078 ± 0.237	-4.035 ± 0.597	M_{xz}	-0.399 ± 0.016	-0.305 ± 0.021	-0.518 ± 0.040
M_{yz}	1.746 ± 0.150	1.273 ± 0.174	2.593 ± 0.548	M_{yz}	0.360 ± 0.014	0.318 ± 0.018	0.441 ± 0.029
ϵ	-0.28 ± 0.02	-0.37 ± 0.03	-0.18 ± 0.16	ϵ	-0.05 ± 0.03	-0.08 ± 0.04	-0.14 ± 0.07
η_P	0.993	1.000	0.942	η_P	0.997	1.000	0.981
η_H	0.974	1.000	0.960	η_H	0.997	1.000	0.976

(Continued on p. 252.)

different depths. The effect of non-linear parameters is not included in the error estimate from the covariance matrix of the moment tensor in the previous section, and may have a strong effect on estimating non-double couple components. We examine this by empirically determining sensitivity of the non-double couple components to the source depth and epicentral location.

TABLE 3(b)

Moment tensor solutions from three moment tensor inversions for intermediate-depth earthquakes

	CMT surface	CMT body	GDSN LP		CMT surface	CMT body	GDSN LP
11 May 1986. NE Taiwan, 200 km, $\epsilon = -0.26 \pm 0.06$				*26 January 1983. Kermadec, 208 km, $\epsilon = -0.40 \pm 0.06$*			
M_0	0.739	0.596	0.803	M_0	3.288	3.087	4.094
M_{xx}	0.024 ± 0.015	0.081 ± 0.021	0.265 ± 0.066	M_{xx}	-0.243 ± 0.095	0.090 ± 0.114	1.963 ± 0.533
M_{yy}	0.410 ± 0.017	0.307 ± 0.025	0.433 ± 0.069	M_{yy}	2.003 ± 0.083	1.447 ± 0.119	1.842 ± 0.321
M_{zz}	-0.435 ± 0.013	-0.388 ± 0.020	-0.698 ± 0.039	M_{zz}	-1.760 ± 0.070	-1.537 ± 0.080	-3.805 ± 0.506
M_{xy}	0.134 ± 0.016	0.174 ± 0.015	0.044 ± 0.062	M_{xy}	0.180 ± 0.083	0.282 ± 0.089	-0.285 ± 0.483
M_{xz}	-0.342 ± 0.010	-0.211 ± 0.017	-0.287 ± 0.025	M_{xz}	-3.191 ± 0.067	-2.954 ± 0.089	-2.875 ± 0.263
M_{yz}	0.506 ± 0.014	0.418 ± 0.019	0.513 ± 0.026	M_{yz}	0.164 ± 0.055	0.071 ± 0.063	-0.107 ± 0.303
ϵ	-0.22 ± 0.02	-0.24 ± 0.02	-0.33 ± 0.07	ϵ	-0.47 ± 0.03	-0.37 ± 0.04	-0.36 ± 0.10
η_P	0.985	1.000	0.953	η_P	0.994	1.000	0.875
η_H	0.981	1.000	0.958	η_H	0.993	1.000	0.950
23 April 1985. Luzon, 181 km, $\epsilon = 0.22 \pm 0.07$				*25 August 1983. Kyushu, 128 km, $\epsilon = 0.20 \pm 0.13$*			
M_0	2.539	1.947	2.390	M_0	0.624	0.529	0.782
M_{xx}	2.564 ± 0.073	2.101 ± 0.072	2.471 ± 0.246	M_{xx}	-0.126 ± 0.014	-0.180 ± 0.015	-0.234 ± 0.050
M_{yy}	-1.042 ± 0.067	-0.825 ± 0.060	-0.965 ± 0.216	M_{yy}	-0.396 ± 0.018	-0.333 ± 0.017	-0.531 ± 0.047
M_{zz}	-1.523 ± 0.044	-1.276 ± 0.050	-1.505 ± 0.169	M_{zz}	0.522 ± 0.018	0.513 ± 0.018	0.766 ± 0.051
M_{xy}	0.690 ± 0.052	0.349 ± 0.055	0.113 ± 0.127	M_{xy}	0.295 ± 0.017	0.099 ± 0.017	0.228 ± 0.060
M_{xz}	-0.905 ± 0.037	-0.751 ± 0.054	-0.752 ± 0.059	M_{xz}	-0.146 ± 0.009	-0.146 ± 0.013	-0.134 ± 0.025
M_{yz}	0.650 ± 0.029	0.295 ± 0.043	0.793 ± 0.100	M_{yz}	-0.245 ± 0.014	-0.276 ± 0.011	-0.324 ± 0.020
ϵ	0.21 ± 0.02	0.30 ± 0.03	0.17 ± 0.06	ϵ	0.07 ± 0.03	0.32 ± 0.03	0.21 ± 0.06
η_P	0.989	1.000	0.974	η_P	0.945	1.000	0.984
η_H	0.986	1.000	0.963	η_H	0.884	1.000	0.957
9 October 1985. Java, 104 km, $\epsilon = 0.21 \pm 0.03$				*24 November 1983. Banda Sea, 183 km, $\epsilon = 0.20 \pm 0.03$*			
M_0	0.347	0.333	0.494	M_0	12.334	15.107	17.625
M_{xx}	-0.028 ± 0.010	0.051 ± 0.012	-0.071 ± 0.035	M_{xx}	-9.735 ± 0.291	-11.853 ± 0.504	-9.786 ± 2.016
M_{yy}	-0.036 ± 0.009	-0.053 ± 0.012	-0.070 ± 0.039	M_{yy}	0.613 ± 0.295	0.407 ± 0.523	-7.834 ± 2.237
M_{zz}	0.065 ± 0.008	0.002 ± 0.009	0.141 ± 0.037	M_{zz}	9.122 ± 0.353	11.446 ± 0.515	17.620 ± 1.921
M_{xy}	0.055 ± 0.011	0.089 ± 0.012	0.026 ± 0.041	M_{xy}	1.732 ± 0.272	4.790 ± 0.546	-4.729 ± 1.983
M_{xz}	0.254 ± 0.007	0.239 ± 0.010	0.353 ± 0.031	M_{xz}	-4.501 ± 0.240	-4.658 ± 0.394	-4.550 ± 0.883
M_{yz}	0.235 ± 0.008	0.223 ± 0.010	0.334 ± 0.026	M_{yz}	-6.866 ± 0.252	-7.328 ± 0.416	-6.849 ± 1.184
ϵ	0.22 ± 0.03	0.24 ± 0.04	0.18 ± 0.10	ϵ	0.23 ± 0.03	0.17 ± 0.04	0.21 ± 0.14
η_P	0.973	1.000	0.939	η_P	0.981	1.000	0.748
η_H	0.984	1.000	0.966	η_H	0.968	1.000	0.492
15 October 1984. Tonga, 80 km, $\epsilon = 0.16 \pm 0.06$				*6 September 1982. S. Honshu, 179 km, $\epsilon = -0.23 \pm 0.04$*			
M_0	4.205	4.060	4.309	M_0	1.695	1.795	2.221
M_{xx}	-2.098 ± 0.085	-0.597 ± 0.104	-1.527 ± 0.382	M_{xx}	0.464 ± 0.045	0.203 ± 0.059	0.838 ± 0.169
M_{yy}	1.753 ± 0.104	0.485 ± 0.143	0.619 ± 0.364	M_{yy}	-0.363 ± 0.049	0.174 ± 0.068	-0.112 ± 0.185
M_{zz}	0.344 ± 0.086	0.113 ± 0.077	0.908 ± 0.573	M_{zz}	-0.101 ± 0.041	-0.377 ± 0.050	-0.726 ± 0.098
M_{xy}	-0.759 ± 0.088	-0.397 ± 0.153	-0.756 ± 0.327	M_{xy}	1.350 ± 0.075	1.251 ± 0.078	1.544 ± 0.232
M_{xz}	-1.125 ± 0.048	-0.916 ± 0.059	-1.067 ± 0.194	M_{xz}	-0.663 ± 0.031	-0.717 ± 0.045	-0.744 ± 0.085
M_{yz}	-3.571 ± 0.084	-3.909 ± 0.104	-3.951 ± 0.209	M_{yz}	0.767 ± 0.036	1.132 ± 0.059	1.241 ± 0.081
ϵ	0.21 ± 0.02	0.08 ± 0.03	0.18 ± 0.10	ϵ	-0.24 ± 0.03	-0.28 ± 0.04	-0.19 ± 0.08
η_P	0.937	1.000	0.977	η_P	0.946	1.000	0.971
η_H	0.938	1.000	0.989	η_H	0.954	1.000	0.975

(Continued on p. 252.)

TABLE 3(a) (continued)

	CMT surface	CMT body	GDSN LP
31 March 1980. S. Honshu, 362 km, $\epsilon = 0.05 \pm 0.13$			
M_0	0.188	0.174	0.237
M_{xx}	0.097 ± 0.010	0.104 ± 0.010	0.103 ± 0.015
M_{yy}	0.019 ± 0.008	-0.027 ± 0.010	-0.026 ± 0.011
M_{zz}	-0.117 ± 0.007	-0.077 ± 0.007	-0.076 ± 0.014
M_{xy}	-0.063 ± 0.007	-0.095 ± 0.007	-0.159 ± 0.019
M_{xz}	-0.139 ± 0.008	-0.115 ± 0.009	-0.146 ± 0.012
M_{yz}	-0.022 ± 0.005	-0.010 ± 0.006	-0.037 ± 0.009
ϵ	-0.08 ± 0.04	0.18 ± 0.05	0.06 ± 0.02
η_P	0.948	1.000	0.976
η_H	0.953	1.000	0.979
7 March 1978. S. Honshu, 441 km, $\epsilon = -0.06 \pm 0.16$			
M_0	4.779	2.782	4.031
M_{xx}	0.755 ± 0.169	0.668 ± 0.142	0.357 ± 0.444
M_{yy}	-2.070 ± 0.260	-1.718 ± 0.231	-1.751 ± 0.343
M_{zz}	1.315 ± 0.123	1.050 ± 0.125	1.394 ± 0.352
M_{xy}	-0.134 ± 0.168	-0.318 ± 0.139	0.885 ± 0.706
M_{xz}	1.415 ± 0.064	0.796 ± 0.128	1.626 ± 0.140
M_{yz}	4.216 ± 0.148	2.245 ± 0.234	3.233 ± 0.348
ϵ	-0.11 ± 0.04	-0.20 ± 0.07	0.12 ± 0.12
η_P	0.981	1.000	0.925
η_H	0.984	1.000	0.917

TABLE 3(b) (continued)

	CMT surface	CMT body	GDSN LP
8 July 1980. Philippine, 185 km, $\epsilon = 0.10 \pm 0.16$			
M_0	0.643	0.856	1.135
M_{xx}	-0.400 ± 0.032	-0.521 ± 0.041	-0.669 ± 0.133
M_{yy}	0.394 ± 0.034	0.201 ± 0.040	0.377 ± 0.128
M_{zz}	0.006 ± 0.022	0.320 ± 0.029	0.293 ± 0.119
M_{xy}	-0.309 ± 0.032	-0.454 ± 0.035	-0.468 ± 0.141
M_{xz}	-0.012 ± 0.017	-0.199 ± 0.025	-0.139 ± 0.070
M_{yz}	-0.425 ± 0.021	-0.533 ± 0.030	-0.858 ± 0.076
ϵ	0.23 ± 0.04	-0.09 ± 0.04	0.15 ± 0.09
η_P	0.909	1.000	0.973
η_H	0.958	1.000	0.976
5 August 1979. Tonga, 204 km, $\epsilon = -0.07 \pm 0.18$			
M_0	0.445	0.386	0.838
M_{xx}	0.021 ± 0.023	0.022 ± 0.033	0.146 ± 0.156
M_{yy}	0.248 ± 0.024	0.136 ± 0.030	0.298 ± 0.116
M_{zz}	-0.269 ± 0.020	-0.158 ± 0.026	-0.444 ± 0.119
M_{xy}	0.006 ± 0.021	-0.117 ± 0.024	-0.129 ± 0.091
M_{xz}	-0.287 ± 0.018	-0.227 ± 0.023	-0.464 ± 0.068
M_{yz}	0.244 ± 0.019	0.252 ± 0.026	0.567 ± 0.052
ϵ	-0.24 ± 0.05	0.11 ± 0.08	-0.09 ± 0.11
η_P	0.925	1.000	0.981
η_H	0.926	1.000	0.985
15 March 1978. Bonin, 278 km, $\epsilon = -0.22 \pm 0.06$			
M_0	0.459	0.388	0.664
M_{xx}	-0.171 ± 0.020	-0.166 ± 0.024	-0.073 ± 0.053
M_{yy}	0.167 ± 0.015	0.174 ± 0.030	0.044 ± 0.048
M_{zz}	0.004 ± 0.012	-0.008 ± 0.016	0.028 ± 0.041
M_{xy}	0.314 ± 0.023	0.250 ± 0.020	0.465 ± 0.057
M_{xz}	-0.222 ± 0.011	-0.145 ± 0.020	-0.176 ± 0.026
M_{yz}	0.229 ± 0.011	0.205 ± 0.018	0.455 ± 0.035
ϵ	-0.29 ± 0.04	-0.17 ± 0.06	-0.21 ± 0.05
η_P	0.991	1.000	0.920
η_H	0.991	1.000	0.922

Unit of M_0 and M_{ij} is $\times 10^{19}$ N m. ϵ at the top of each table represents the average value and the standard deviation of the three solutions. The coordinates of the axes follow the definition of Nábělek (1984). η_P and η_H represent the resemblance in radiation pattern of P and SH waves, respectively, which are computed using eqn. (5).

3.4.1. Source depth

Figure 4(a) shows the dependence of ϵ on the centroid depth in the CMT body wave and surface wave inversions for the 1 January 1984 South of Honshu earthquake (Kuge and Kawakatsu, 1990). The solid stars correspond to the solutions for the centroid depth (h_c) and ϵ from the full CMT inversion in which the centroid depth is one of the unknown parameters. Solid circles are ϵ from CMT inversions in which the centroid depths are fixed. The open stars and open circles represent the variance reduction between observed and synthetic waveforms given by

$$\frac{\sum_j w_j^2 \left[\sum_i \left(s_{ij}^{\mathrm{obs}}\right)^2 - \sum_i \left(s_{ij}^{\mathrm{obs}} - s_{ij}^{\mathrm{syn}}\right)^2 \right]}{\sum_j w_j^2 \sum_i \left(s_{ij}^{\mathrm{obs}}\right)^2} \times 100(\%) \tag{3}$$

where s_{ij}^{obs}, s_{ij}^{syn}, and w_j are observed seismograms, synthetic seismograms, and weighting factors, respectively, and the subscript ij corresponds to the ith data point of the jth waveform. When the synthetic waveforms are the same as the observations, the value is 100. As Fig. 4(a) shows, although the variance reductions do not change much with the assumed depth, ϵ is almost constant. For the other earthquakes, ϵ also does not vary much, especially for ϵ estimated by the CMT inversions of surface waves. In cases with the depth fixed at $h_c - 20$ km or $h_c + 20$ km, usually the variation of ϵ is about 0.02, and not larger than 0.07. The average discrepancy be-

tween the International Seismological Center (ISC) or Preliminary Determination of Epicenters (PDE) depth and the centroid depth (h_c) from the CMT inversion is about 10 km. Over such a depth range, ϵ is stable and the sign does not change.

Figure 4(b) shows ϵ vs. source depth for the 23 April 1985 Luzon intermediate-depth event for GDSN LP inversions. ϵ does not vary much (± 0.01), even if the depth increases or decreases by 20 km from our preferred depth. For the other events, except for the 26 January 1983 Kermadec event, the variation of ϵ for 10 km fluctuations in depth is not large enough for ϵ to become zero. For deep events, an ϵ value does not depend on the change in the source depth because we separately model P and pP waveforms without absolute time information (GDSN LP inversion).

3.4.2. Epicentral location

Figure 5 shows the effect of the source location on ϵ for the same event as in Fig. 4(a). The location is shifted in the longitudinal or latitudinal directions from the centroid location (lat_c, long_c) obtained through the full CMT inversion in which the centroid location, including the depth, is an unknown parameter. We fix the centroid depth. The open and solid stars correspond to the variance reduction and ϵ at the centroid location from the full CMT inversion, respectively. The horizontal axis shows the assumed location, which is represented by the departure (in degrees) from the centroid location. The solid circles indicate the ϵ at shifted locations. The average discrepancy between the ISC or PDE location and the centroid location from the full CMT inversion is about 0.4°. For such

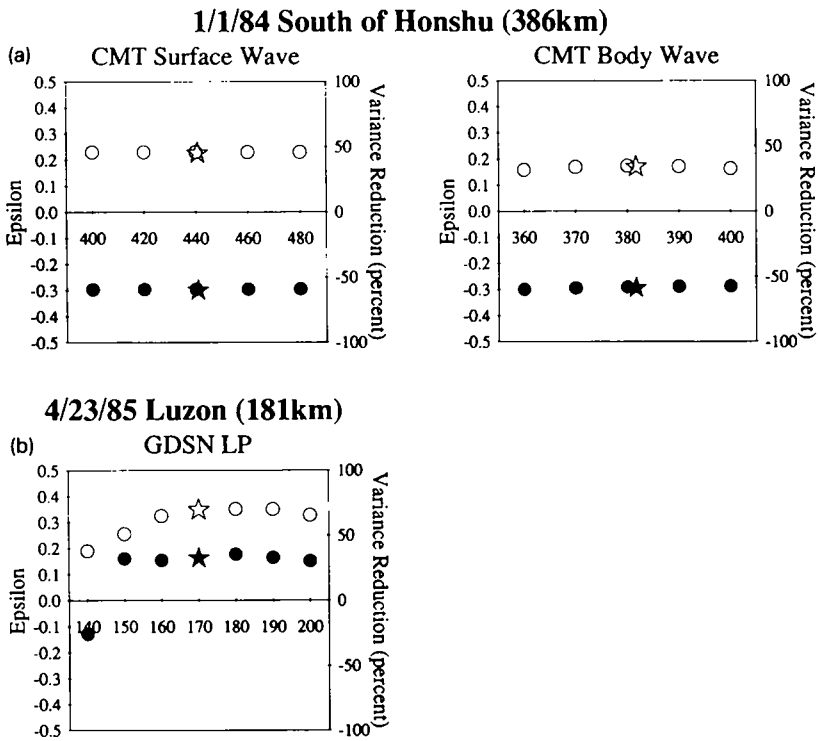

Fig. 4. Dependence of non-double couple components (ϵ) on the source depth. The horizontal axis represents the centroid depth assumed in each inversion. Solid stars and solid circles represent ϵ. The variance reduction (%) between the observed and synthetic waveforms, following eqn. (3), are shown by an open star and open circles. (a) Results for the 1 January 1984 South of Honshu deep earthquake in CMT inversions. Stars correspond to the solution in a full CMT inversion in which the centroid depth is one of the unknown parameters. (b) Results for the 23 April 1985 Luzon intermediate-depth earthquake in GDSN LP inversions. Stars correspond to our solution with the maximum variance reduction.

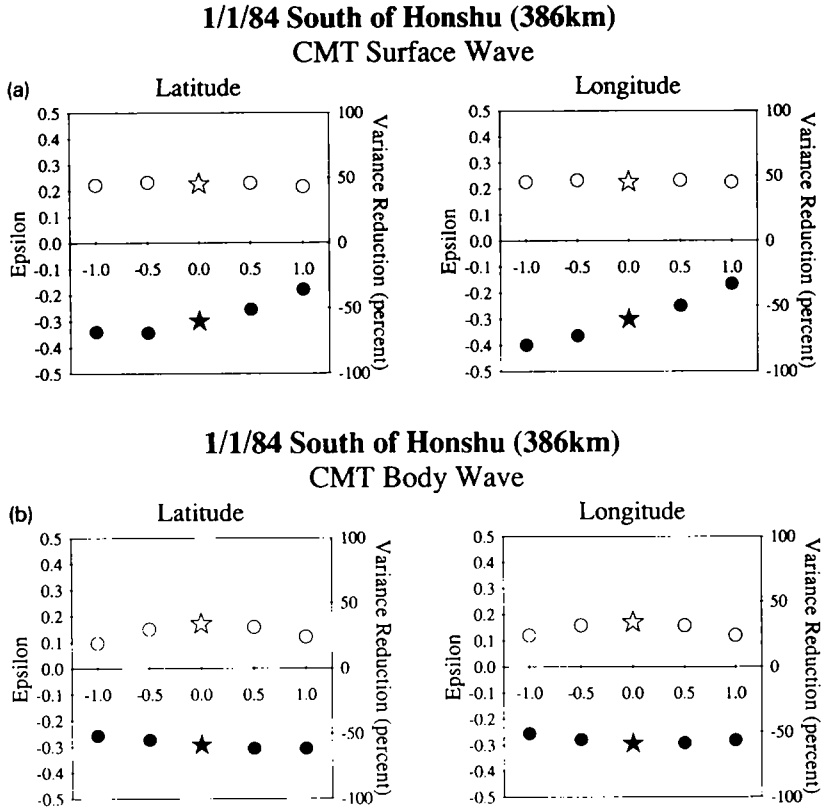

Fig. 5. Dependence of non-double couple components (ϵ) on the source location in CMT inversions for the 1 January 1984 South of Honshu deep earthquake. The source location is moved in a longitudinal or latitudinal direction. A horizontal axis shows the location fixed in the inversion, which is represented by the departure (in degrees) from the centroid location. The centroid depth is also fixed. A solid star and solid circles represent ϵ. The variance reductions (%) from (3) are also shown by an open star and open circles. Stars correspond to the solution in a full CMT inversion in which the centroid location is an unknown parameter. (a) CMT inversions of surface waves; (b) CMT inversions of long-period body waves.

changes of the locations, ϵ in Fig. 5 varies by less than 0.05 and there is some decrease in variance reduction (open circles). It is unlikely that ϵ becomes zero or that the sign of ϵ changes as a result of error in the epicentral location. For most of the other earthquakes, when the source is located within $\text{lat}_c \pm 0.5°$ and $\text{long}_c \pm 0.5°$, the variation in ϵ is less than 0.08 and the sign of ϵ does not change. For CMT inversions of surface waves, ϵ values for the 7 March 1978 South of Honshu event show a change in sign as the location is moved by 0.5°. For CMT inversions of long-period body waves, the signs of ϵ for the 8 July 1980 Philippine, Bonin, 15 October 1984 Tonga, and 24 November 1983 Banda Sea events change. For the Tonga event, the change in sign is accompanied by significant decrease in variance reduction. For the other three events, however, the decrease in variance reduction is not so significant, less than 10%, so in those cases ϵ seems to be unstable for changes in location.

4. Discussion

4.1. Benefit of comparing three moment tensor solutions

Comparison of the three solutions allows us to judge the stability of the non-double couple com-

ponent for each event. We use various seismic waves in different frequency bands in the three inversions. If some inconsistency is observed between the three solutions, we can infer that the origins of the non-double couple components may exist in the inversion procedure (e.g. effect of unmodeled propagation errors).

The different seismic waves also give different intrinsic resolvability of the moment tensor. These differences can be seen in the correlation matrix for the moment tensor. Figure 6 shows the correlation matrix of the 1 January 1984 South of Honshu deep earthquake. The correlation matrix is computed from the covariance matrix. The coordinates for the moment tensor components are rotated to isolate an isotropic part of the moment tensor so that $C = (M_{\theta\theta} + M_{\phi\phi} - 2M_{rr})/3$ and $D = (M_{\theta\theta} - M_{\phi\phi})/2$. As the isotropic component is set to be zero, only five components are shown. The open and solid circles correspond to positive and negative correlations, respectively. The size of the circle represents the strength of the correlation. Strong correlations appear between different moment tensor components in different inversions. For the CMT inversion of surface waves, a negative correlation between C and D is significant. For the GDSN LP inversion, a strong negative correlation appears between D and $M_{r\theta}$. The value below each correlation matrix is the condition number of the normal equation in the inverse problem for the moment tensor, which is the ratio between the minimum and maximum eigenvalues of the kernel in the normal equation. The values vary in the three inversions. Three moment tensors are thus independently estimated for each event with different resolvability.

4.2. *Resemblance of radiation pattern*

Similarity of ϵ alone does not guarantee that the non-double couple component is resolved in a self-consistent manner. It is possible that two moment tensor estimates have the same ϵ but totally different focal mechanisms. To quantify the similarity of focal mechanisms of two moment tensors, we compare the bodywave radiation patterns.

Radiation patterns ($R(\xi, \psi)$) of P and S waves can be represented in terms of normalized spherical harmonics ($Y_l^m(\xi, \psi)$):

$$R_P(\xi, \psi) = \sum_{l,m} A_{lm} Y_l^m \tag{4a}$$

$$R_{SV}(\xi, \psi) = -0.5 \sum_{l,m} A_{lm} \frac{\partial Y_l^m}{\partial \xi} \tag{4b}$$

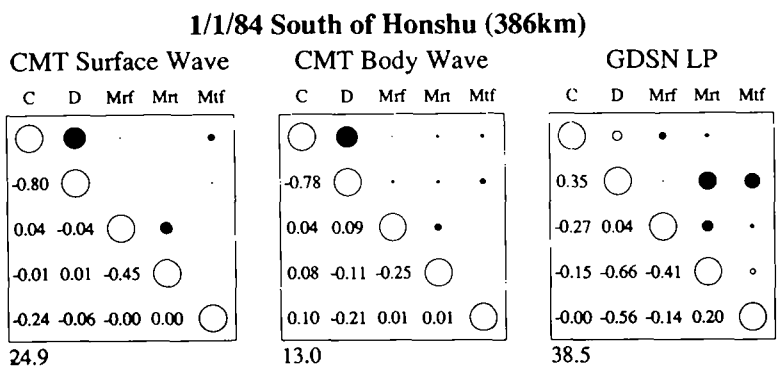

Fig. 6. Correlation matrix of moment tensor components for the 1 January 1984 South of Honshu deep earthquake. Open and solid circles show positive and negative correlation, respectively. The size of a circle on the upper side represents the strength of correlation between two components. The values of the correlation matrix are also shown on the lower side. The coordinates for the moment tensor components are rotated to isolate an isotropic part of moment tensor, such that $C = (M_{\theta\theta} + M_{\phi\phi} - 2M_{rr})/3$, $D = (M_{\theta\theta} - M_{\phi\phi})/2$, $M_{rt} = M_{r\theta}$, $M_{rf} = M_{r\phi}$, and $M_{tf} = M_{\theta\phi}$, where the coordinates r, θ, and ϕ follow Dziewonski and Woodhouse (1983a, b). A condition number of the normal equation for the moment tensor is presented below each box.

TABLE 4

Coefficients for the comparison of radiation patterns

	$l=0$ $m=0$	$m=0$	$l=2$ $m=\pm 1$	$m=\pm 2$
A_{lm}	$2(\pi)^{1/2}I$	$-\frac{2(\pi)^{1/2}}{(5)^{1/2}}C$	$-\frac{2(2\pi)^{1/2}}{(15)^{1/2}}[\pm M_{r\theta}+iM_{r\phi}]$	$\frac{2(2\pi)^{1/2}}{(15)^{1/2}}[D\pm iM_{\theta\phi}]$
B_{lm}	0	0	$-\frac{2(2\pi)^{1/2}}{(15)^{1/2}}[\pm M_{r\theta}+iM_{r\phi}]$	$\frac{2(2\pi)^{1/2}}{(15)^{1/2}}[D\pm iM_{\theta\phi}]$

$I=(M_{rr}+M_{\theta\theta}+M_{\phi\phi})/3$, $C=(M_{\theta\theta}+M_{\phi\phi}-2M_{rr})/3$, and $D=(M_{\theta\theta}-M_{\phi\phi})/2$.

$$R_{SH}(\xi,\psi)=0.5\sum_{l,m}A_{lm}\frac{1}{\sin\xi}\frac{\partial Y_l^m}{\partial\psi} \qquad (4c)$$

where $l=0$, 2, and $|m|\le 2$ and A_{lm} are shown in Table 4. ξ and ψ correspond to take-off angle and azimuth, respectively. The similarity of two focal mechanisms may be obtained by calculating the cross-correlation of corresponding radiation patterns. Because of the orthonormality of the spherical harmonics, the cross-correlation is equal to the cross-correlation of the coefficients given

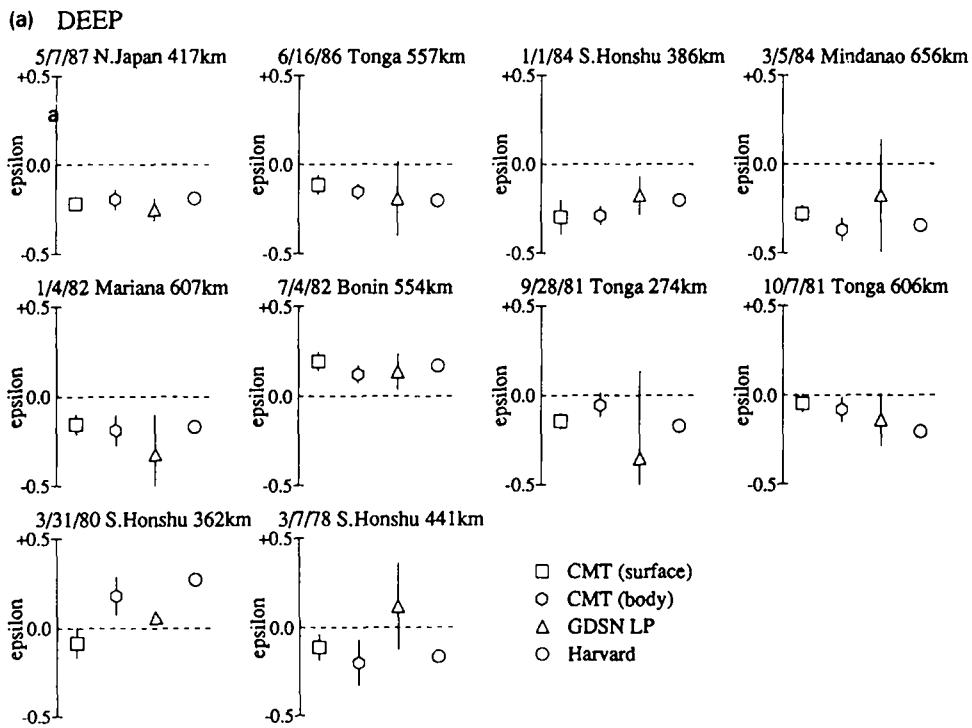

Fig. 7. Non-double couple components (ϵ) from different moment tensor inversions. The bars for the ϵ ranges are estimated using the perturbation approach ($\epsilon\pm 2\Delta\epsilon$; see eqn. (2)). The ϵ of the Harvard CMT solution is also shown (Dziewonski et al., 1983a, b, 1984a–c, 1985, 1986a, b, 1987a–c, 1988a–c). (a) Deep earthquakes; (b) intermediate-depth earthquakes.

(b) Intermediate-depth

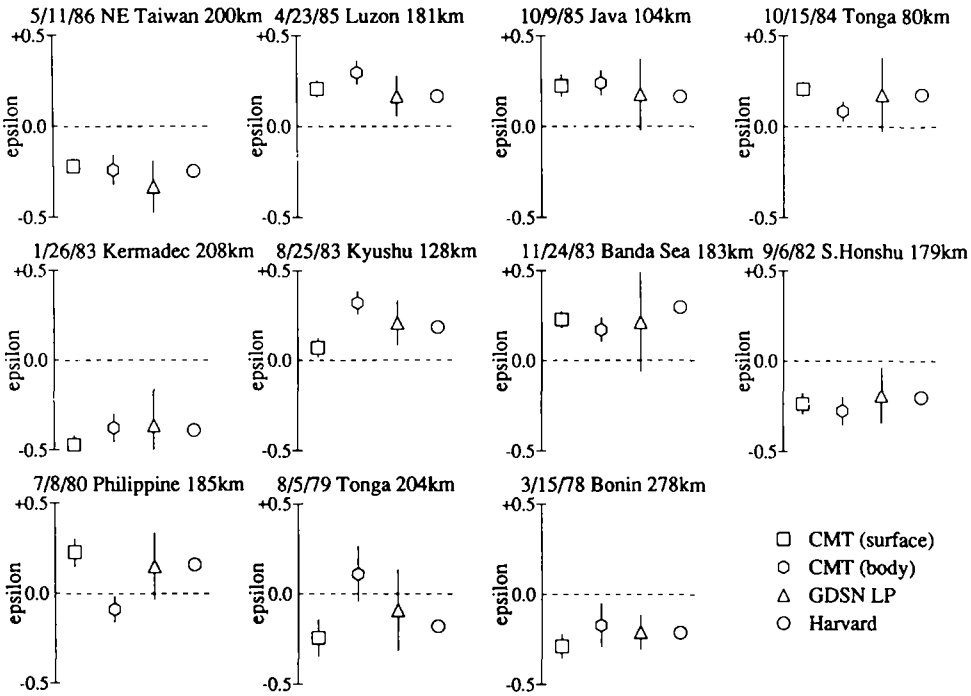

Fig. 7 (continued).

in (4). We thus compute the correlation between two sets of coefficients and compare two radiation patterns by

$$\eta_P = \frac{\sum_{l,m} (A_{lm})_1 (A_{lm})_2}{\left[\sum_{l,m} (A_{lm})_1 (A_{lm})_1^*\right]^{1/2} \left[\sum_{l,m} (A_{lm})_2 (A_{lm})_2^*\right]^{1/2}} \quad (5a)$$

$$\eta_H = \frac{\sum_{l,m} (B_{lm})_1 (B_{lm})_2}{\left[\sum_{l,m} (B_{lm})_1 (B_{lm})_1^*\right]^{1/2} \left[\sum_{l,m} (B_{lm})_2 (B_{lm})_2^*\right]^{1/2}} \quad (5b)$$

where the subscripts 1 and 2 correspond to two different moment tensor solutions, and B_{lm} corresponds to the effective parts of A_{lm} for SH waves (Table 4). The values of η_P and η_H are one if the radiation patterns are the same.

The results of η are shown in Table 3. We compute η between the solutions from CMT inversions of surface waves and long-period body waves, and η between the solutions from CMT inversions of long-period body waves and GDSN LP inversions. For the 24 November 1983 Banda Sea event, the η values involving the GDSN LP inversion are exceptionally low. The moment tensor solution from the isolated body wave inversion is different from the other two solutions; this difference may be caused by the small number of available body wave data (Kuge, 1991). For the other events, however, most η are greater than 0.9, which suggests that the moment tensor solutions from different inversions are generally similar, and therefore the consistency of ϵ from the three inversion schemes may be taken as evidence for the true similarity of the non-double couple components of those moment tensors.

4.3. *Comparison of non-double couple components*

Non-double couple components (ϵ) from our three moment tensor inversions for the 21 inter-

mediate-depth and deep events are shown in Fig. 7, along with ϵ from the Harvard CMT solutions. For events before 1981, the sign of ϵ often changes in different inversions (the 7 March 1978 South of Honshu, 31 March 1980 South of Honshu, 5 August 1979 Tonga, and 8 July 1980 Philip-

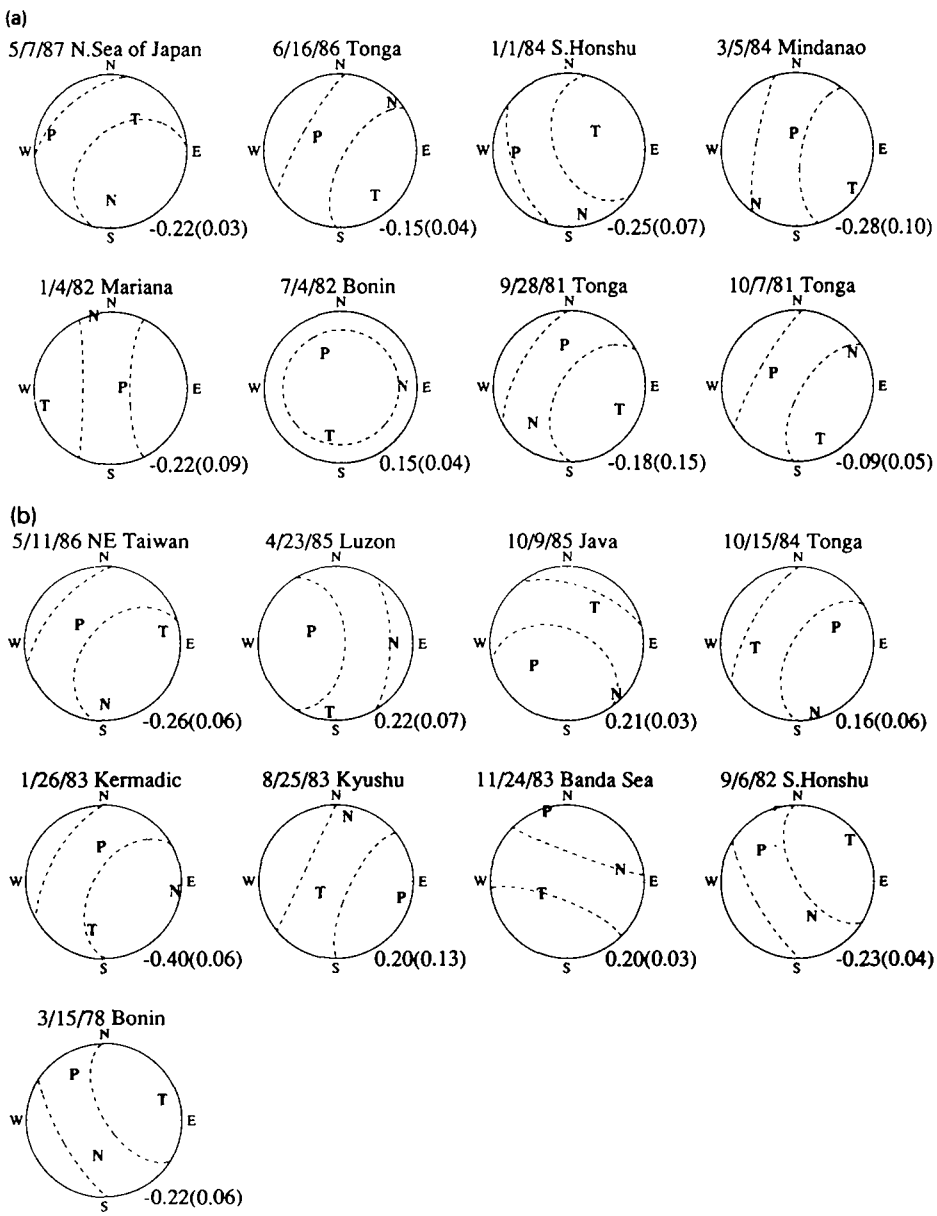

Fig. 8. Principal axes of non-double couple earthquakes and the directions of the subducting slabs. We present only the earthquakes whose non-double couple components (ϵ) have the same sign in our three different inversions (Fig. 7). The value below the focal sphere represents the average ϵ from the three moment tensor solutions and the number in parentheses is the standard deviation. The dotted lines represent the range of planes which are parallel to the slab and within 25° of the dip angle of the slab on the unit focal sphere. (a) Deep earthquakes; (b) intermediate-depth earthquakes. The 4th July 1982 Bonin event occurred isolated from the Wadatio–Benioff zone, but a horizontally lying slab is assumed following Okino et al. (1989).

pine events). This may reflect the limited data availability immediately after the GDSN network started to operate and/or the lack of appropriate station coverage.

Of 21 events, 17 events show consistent signs of ϵ in the three different solutions. Those 17 events are given in Table 2. It is unlikely that the consistent non-double couple components are caused by unmodeled propagation errors, limited station coverage, or instability of the inversion procedures. A few moment tensor solutions do seem to be dependent on the source location and the seismic data in the inversion procedures (26 January 1983 Kermadec and 24 November 1983 Banda Sea events). Nevertheless, such effects are not enough for ϵ to change sign for the other events. Allowing for the error bars, the magnitudes of ϵ are also consistent. Figure 7 thus suggests that the non-double couple components are actual characteristics of the seismic radiation, by the sources themselves, or by structures very close to the source areas.

The non-double couple components show a correlation with strain release within slabs. Figure 8 indicates the principal axes of the 17 non-double couple events for which we observe consistent signs of ϵ in the three moment tensor inversions. The principal axes are determined from the CMT inversions of long-period body waves (Table 3). The dotted lines represent the range of planes which are parallel to the slab and within 25° of the dip angle of the slab on the unit focal sphere. Fujita and Kanamori (1981) defined 'in-plate stress' events as those whose principal axes are in a similar range. The value below each circle gives the average ϵ from the three moment tensor inversions, with the standard deviation in parentheses. ϵ is negative when the compressional (P) axis is within the subducting slab, whereas ϵ is positive when the tensional (T) axis is within the slab. For each event, except for the 4 July 1982 Bonin isolated event, the principal strain within the slab is consistent with the inclined axes of other events within the same slab (Table 1). Within regions of slabs with predominantly tensional strain release, the tensional principal strain in each moment tensor is predominant, that is, $\epsilon > 0$, whereas the compressional principal strain

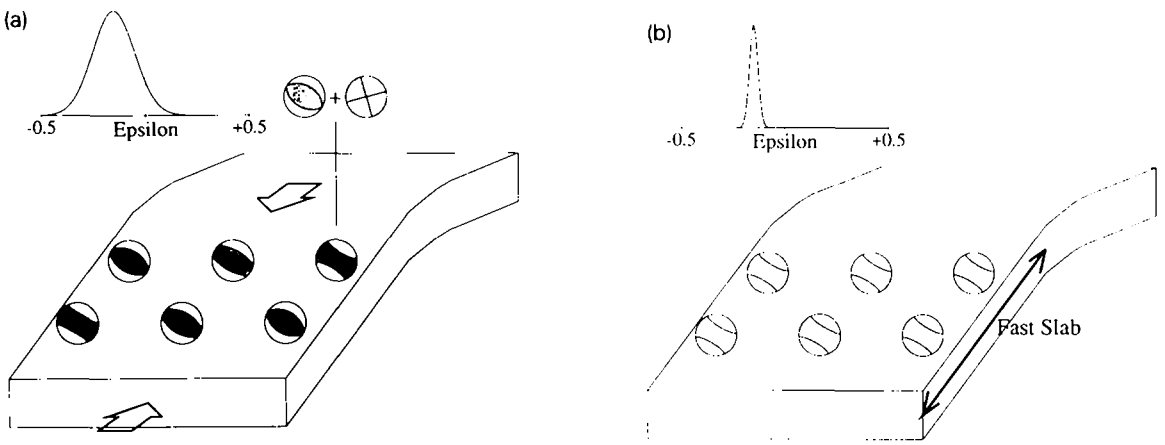

Fig. 9. Possible origins of non-double couple components in response to the state of strain release within slabs. A case of predominant down-dipping compressional strain release is shown. Within slabs of predominant tensional strain release, the P and T axes of the moment tensors are exchanged with each other, and positive ϵ tends to be observed. (a) Complexity in source process. Non-double couple components result from the combination of subevents with different double couple mechanisms. Of the principal axes of the subevent mechanisms, one principal axis, which exists within the dipping slab, appears in the same direction in different subevent mechanisms, whereas the other two axes rotate around the direction of the stable principal axis (Kuge and Kawakatsu, 1990, 1992). (b) Presence of high-velocity slab. The velocity is relatively high in the directions within slabs, whereas the velocity is relatively low in the direction perpendicular to the slabs. The anisotropic effect around the source results in non-double couple components in relation to the principal axes within the slabs. The expected non-double couple components are systematic within the same slab.

in the moment tensor becomes significant, that is, $\epsilon < 0$, within regions of slabs under compressional strain release. The correlation observed as the statistical nature of non-double couple components (Figs. 1 and 2) seems to be the case for the moment tensor of each event which exhibits a significant non-double couple component.

4.4. *Possible causes of non-double couple components*

4.4.1. *Complexity in source process*

Analyses of very broadband seismic waveforms by Kuge and Kawakatsu (1990, 1992) suggest that significant non-double couple components of moment tensors can be caused by the superposition of different double couple sources. For two large non-double couple earthquakes, Kuge and Kawakatsu found that the source processes are composed of two interfering arrivals with relative amplitude or polarity varying from station to station. The separate double couples of the two subevents combine to produce the significant non-double couple components obtained at long periods (Fig. 9(a)). Of the principal axes of the subevent mechanisms, one principal axis, within the dipping slab, was found to have the same direction in the different subevent mechanisms, whereas the other two axes rotate around the direction of the stable principal axis. This multiple event mechanism, if common, can explain the observation of a relationship between non-double couple components and the predominant strain release within the subducting slabs as discussed by Kuge and Kawakatsu (1992), and is also consistent with the lack of significant isotropic components of deep events (Kawakatsu, 1991a, 1992).

4.4.2. *Effect of high-velocity slab*

The presence of the high-velocity slab causes the velocity of seismic waves to be relatively high in directions within the slab, whereas it is relatively low in the direction perpendicular to the slab (Fig. 9(b)). For long-period seismic waves, we may consider this effect as the existence of an anisotropic medium around the source. Figure 10(a) shows the distortion of the P wave nodal surfaces in a case where the double couple source is in an anisotropic medium. The nodal planes of the original source are perpendicular to each

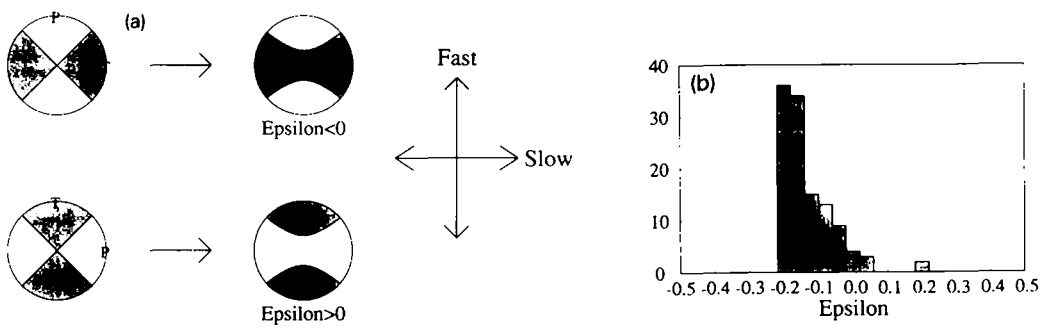

Fig. 10. Effect of the presence of high-velocity slabs. (a) P-wave radiation patterns of double couple sources in an anisotropic media. The radiation pattern is obtained for the moment tensor, $M_{ij} = [u_k]\, \nu_l C_{klij}$, where u is relative displacement on a fault, ν is the direction normal to the fault plane, and C_{klij} represents elastic constants. Elastic constants for a single crystal of olivine (Kumazawa and Anderson, 1969) are used for C_{klij}. 'Fast' and 'Slow' directions correspond to the a-axis and b-axis of the crystal, respectively. An isotropic component is removed from the resultant moment tensor; that is, the component (I) is forced to be zero (see the text). (b) Histogram of non-double couple components (ϵ) expected for double couple sources in a medium that has high velocity in the direction of the subducting slab. The non-double couple components are computed from the equation in (a). We use double couple mechanisms of events in Tonga (depth 100 km or greater, log M_0[N m] $\geq$ 17.5) in the Harvard CMT solutions. For C_{klij}, we rotate the elastic constants of Kumazawa and Anderson (1969) so that the c-axis is N30°E in the horizontal plane, and the a-axis is in the direction of the subducting slab, whose dip and strike angles are 60° and N60°W, respectively. An isotropic component is removed from the moment tensor. As the compressional axes of the events and the direction of high velocity are close to each other, a shift of ϵ to the negative side is observed. The variance of the ϵ distribution is small.

other, though the nodal surfaces that we observe in the anisotropic medium are no longer perpendicular. Although some isotropic components are expected in the radiation patterns for the anisotropic medium, they should have little effect on the results in CMT inversions under the constraint that $I = (M_{rr} + M_{\theta\theta} + M_{\phi\phi})/3 = 0$. This is because the isotropic components are well isolated from the other components of a moment tensor in the estimation procedure, especially for CMT inversions of deep events using long-period body waves (Kawakatsu, 1991a, 1992). We calculated synthetic waveforms from isotropic sources at depths from 100 to 650 km, and performed CMT inversions under the constraint that $I = 0$. The results of this simulation suggest that less than 15% of the isotropic source is observed as a vertical CLVD component (C) in the deviatoric moment tensor solution in the body wave CMT inversions. Even for the surface wave CMT inversions, no more than 30% appears as C. For Fig. 10(a), we thus remove the isotropic components from the resultant moment tensors; that is, $I = 0$. When the compressional principal axis of the double couple source is in the fast direction of the anisotropic medium, the moment tensor is observed to show a negative non-double couple component ($\epsilon < 0$), whereas we observe positive ϵ when the tensional axis is aligned with the fast direction of the medium. Judging from this, high-velocity slabs may be responsible for the relationship of non-double couple components with principal strain axes that appear within the slabs.

As seismic mechanisms of intermediate-depth and deep earthquakes are generally similar, reflecting the state of predominant compressional or tensional strain release within a slab, non-double couple components expected from the presence of high-velocity slabs should be systematic within the slab. Figure 10(b) shows a histogram of the non-double couple components expected for double couple sources in a medium that has relatively high velocity in the direction of the subducting slab. The non-double couple components are computed from moment tensors simulated by $M_{ij} = [u_k]\nu_l C_{klij}$, where $\boldsymbol{u}$ is relative displacement on a fault, $\boldsymbol{\nu}$ is the direction normal to the fault plane, and C_{klij} represents elastic constants around the fault plane. For $\boldsymbol{u}$ and $\boldsymbol{\nu}$, we use the best double couple mechanisms of Harvard CMT solutions for intermediate-depth and deep events in Tonga, for which the compressional principal axes are well aligned with the subducting direction. For C_{klij}, we assume the elastic property of single crystal olivine (Kumazawa and Anderson, 1969) for which the fast crystal axis (a-axis) is aligned with the subduction direction. Isotopic components are removed from the resultant moment tensors. Because the compressional principal axes and the direction of high velocity in the assumed media are close to each other, we observe a large shift of ϵ to the negative side, and the variance of ϵ is small.

4.4.3. Which is more responsible?

For significant ϵ (e.g. the 6 September 1982 Bonin and 11 May 1986 NE Taiwan events), complexity in the source process is more likely to be responsible than the presence of a high-velocity slab. Even considering the error ranges of ϵ, the large values of ϵ appear to be near the edge of the ϵ distribution for the events within the same slab, and rather rare (Fig. 1 and Table 1). The directions of the principal strain axes for these events are not exceptional, being consistent with those for the other events within the same slab. If the large ϵ is caused by the high-velocity slab, most of the other events should also show large ϵ, but this is not the case. The slab heterogeneity is not sufficient to explain that significant ϵ resulted from a wide distribution of ϵ (Fig. 9).

Figure 11 shows the broadband P-wave displacement waveforms of the non-double couple events shown in Fig. 8. For the 1 January 1984 South of Honshu and 23 April 1985 Luzon events, Kuge and Kawakatsu (1990, 1992) showed that the existence of subevents with different double couple mechanisms causes the significant non-double couple components. For the 6 September 1982 South of Honshu and 26 January 1983 Kermadec events, we observe polarity changes during the source process at stations near the nodal planes. For the 11 May 1986 NE Taiwan event, several subevents appear. The large non-double

couple components could be caused by changes in the focal mechanisms. For earthquakes with simple displacement waveforms (e.g. the 4 January 1982 Mariana event), the change in focal mechanism could occur with short or no time delay so that we cannot observe waveform complexity.

For the systematic shift of ϵ in Figs. 1 and 2,

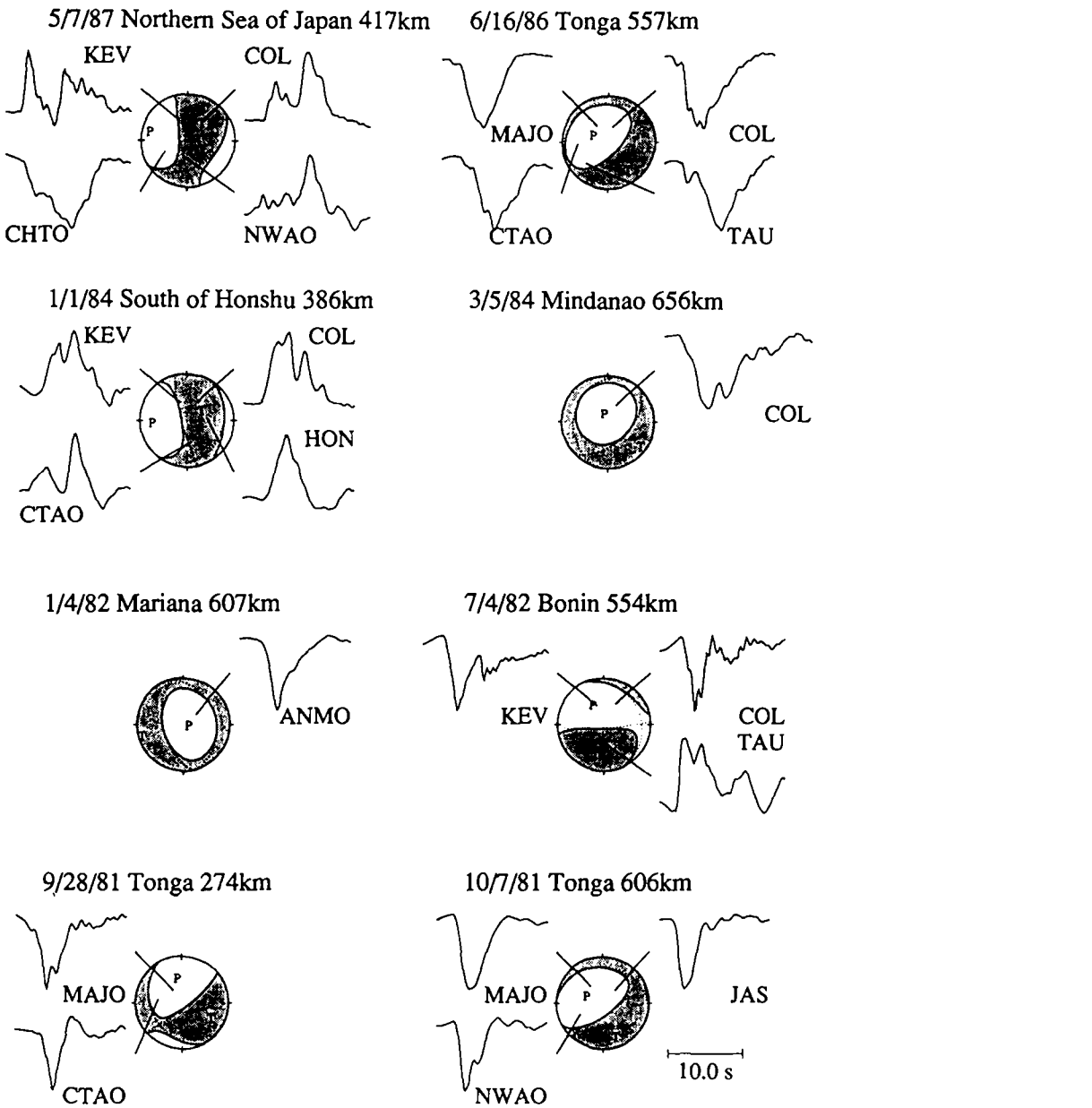

Fig. 11. Broadband P-wave displacement waveforms of the non-double couple earthquakes. The earthquakes are the same as for Fig. 8. The moment tensor solutions from the CMT inversions of long-period body waves are shown. All seismograms are shown on the same time-scale.

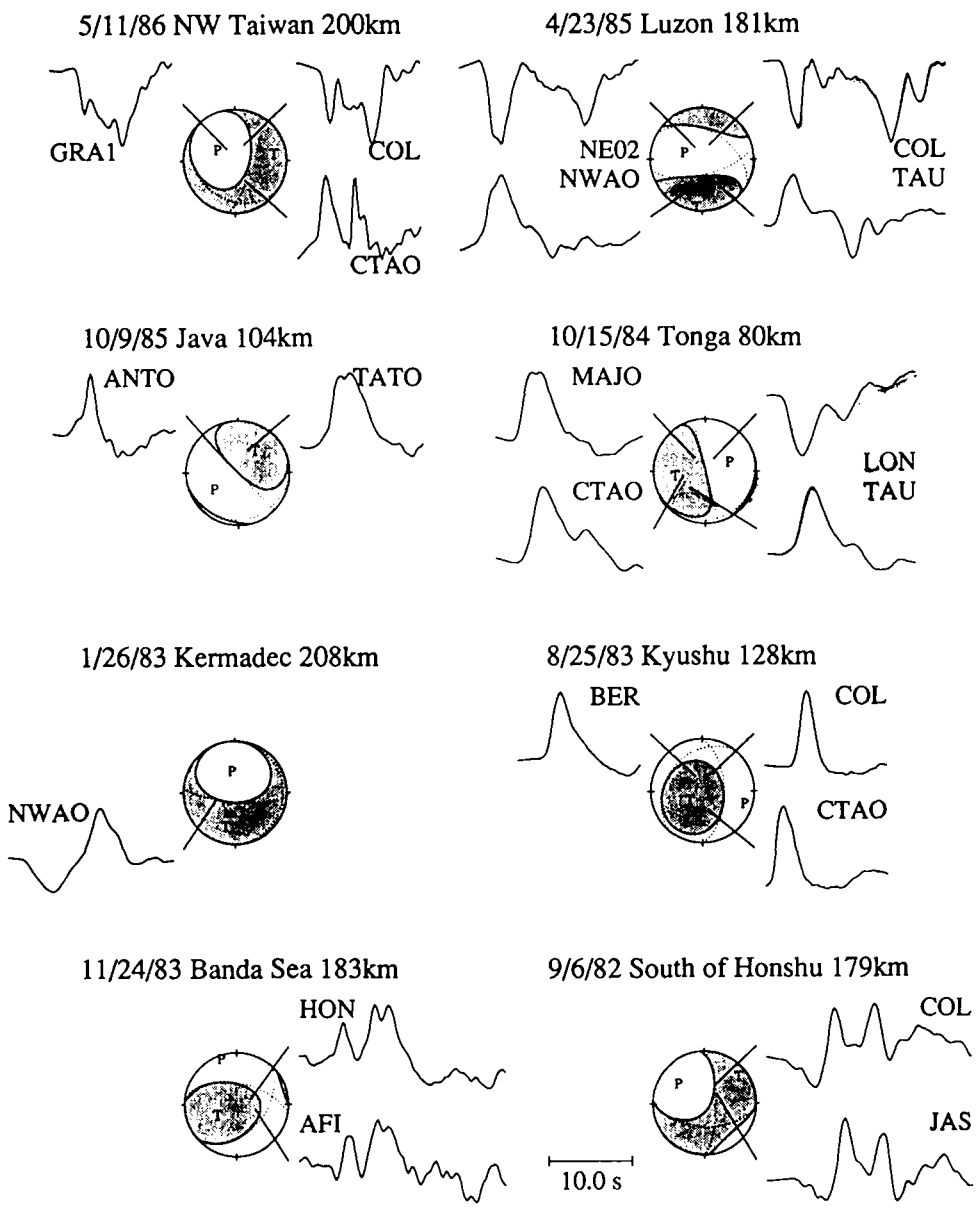

Fig. 11 (continued).

or the non-double couple components of events that are similar in value to the ϵ distribution of the other events within the same slab (Table 1), it is noted that the effect of subducting slabs may still explain the non-double couple components. Figure 12 shows the dependence of ϵ on the

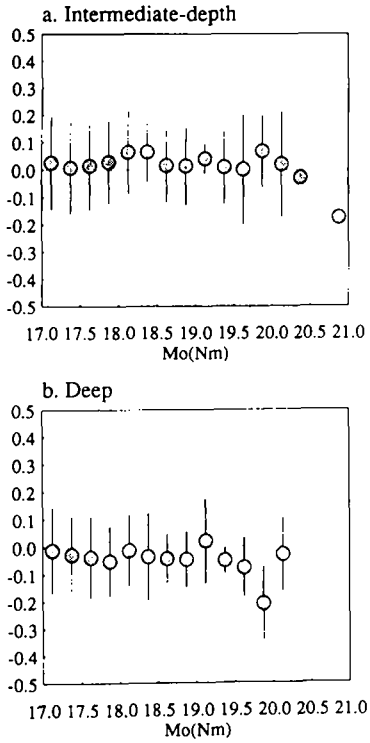

Fig. 12. Dependence of non-double couple components (ϵ) on the seismic moment. The vertical bar corresponds to 1 s.d. The Harvard CMT solutions during the period between 1977 and January 1991 are used. (a) Intermediate-depth earthquakes; (b) deep earthquakes.

seismic moment. For both deep and intermediate-depth events, a systematic shift in the ϵ value tends to appear, independent of the seismic moment. The effect of subducting slabs might provide a good explanation for this observation, whereas if the systematic shift in ϵ is caused by complexity in the source, the complexity should be independent of the seismic moment.

As discussed by Knopoff and Randall (1970) and Kuge and Kawakatsu (1992), change of the elastic property in a source volume (for example, because of phase transition) can cause a non-double couple component in the seismic radiation. Our discussions, however, imply that the existence of such intrinsic non-double couple sources is not inevitable to explain the non-double couple behaviors of deep and intermediate-depth earthquakes.

5. Conclusion

Analyses of non-double couple intermediate-depth and deep earthquakes using three inversions of different seismic waves at long periods indicate that significant non-double couple components exist in the source moment tensors in response to the state of predominant strain release within the slabs. The non-double couple components are likely to be caused by complexity in source process or near-source slab structures.

Acknowledgments

We thank L. Hwang, S. Watada, and M. Zirbes for helping us to collect the old and recent GDSN data. We thank T. Lay for reviewing the manuscript. Completion of this work at UCSC was partially supported by NSF Grant EAR-8451715 and the W.M. Keck Foundation, and K.K. received support from the Japan Society for the Promotion of Science. This paper is Contribution 170 of the Institute of Tectonics and C.F. Richter Seismological Laboratory at the University of California, Santa Cruz.

References

Barker, J.S. and Langston, C.A., 1983. A teleseismic body wave analysis of the May 1980 Mammoth Lakes, California, earthquakes. Bull. Seismol. Soc. Am, 73: 419–434.

Burnley, P.C., Green, II, H.W. and Prior, D.J., 1991. Faulting associated with the olivine to spinel transformation in Mg_2GeO_4 and its implications for deep-focus earthquakes. J. Geophys. Res., 96: 425–553.

Doornbos, D.J., 1985. Source solutions and station residuals from long-period waveform inversion of deep events. J. Geophys. Res. 90: 5466–5478.

Dziewonski, A.M. and Anderson, D.L., 1981. Preliminary reference Earth model. Phys. Earth Planet. Inter., 25: 297–356.

Dziewonski, A.M. and Woodhouse, J.H., 1983a. Studies of the seismic source using normal-mode theory. In: H. Kanamori

and E. Boschi (Editors), Earthquakes: Observation, Theory and Interpretation. North-Holland, Amsterdam, pp. 45–137.

Dziewonski, A.M. and Woodhouse, J.H., 1983b. An experiment in systematic study of global seismicity: centroid-moment tensor solutions for 201 moderate and large earthquakes in 1981. J. Geophys., Res., 88: 3247–3271.

Dziewonski, A.M., Chou, T.A. and Woodhouse, J.H., 1981. Determination of earthquake source parameters from waveform data for studies of global and regional seismicity. J. Geophys. Res., 86: 2825–2852.

Dziewonski, A.M., Friedman, A., Giardini, A. and Woodhouse, J.H., 1983a. Global seismicity of 1982: centroid-moment tensor solutions for 308 earthquakes. Phys. Earth Planet. Inter., 33: 76–90.

Dziewonski, A.M., Friedman, A. and Woodhouse, J.H., 1983b. Centroid-moment tensor solutions for January–March 1983. Phys. Earth Planet. Inter., 33: 71–75.

Dziewonski, A.M., Franzen, J.E. and Woodhouse, J.H., 1984a. Centroid-moment tensor solutions for July–September 1983. Phys. Earth Planet. Inter., 34: 1–8.

Dziewonski, A.M., Franzen, J.E. and Woodhouse, J.H., 1984b. Centroid-moment tensor solutions for October–December 1983. Phys. Earth Planet. Inter., 34: 129–136.

Dziewonski, A.M., Franzen, J.E. and Woodhouse, J.H., 1984c. Centroid-moment tensor solutions for January–March 1984. Phys. Earth Planet. Inter., 34: 209–219.

Dziewonski, A.M., Franzen, J.E. and Woodhouse, J.H., 1985. Centroid-moment tensor solutions for October–December 1984. Phys. Earth Planet. Inter., 39: 147–156.

Dziewonski, A.M., Franzen, J.E. and Woodhouse, J.H., 1986a. Centroid-moment tensor solutions for April–June 1985. Phys. Earth Planet. Inter., 41: 215–224.

Dziewonski, A.M., Franzen, J.E. and Woodhouse, J.H., 1986b. Centroid-moment tensor solutions for October–December 1985. Phys. Earth Planet. Inter., 43: 185–195.

Dziewonski, A.M., Ekström, G., Franzen, J.E. and Woodhouse, J.H., 1987a. Centroid-moment tensor solutions for April–June 1986. Phys. Earth Planet. Inter., 45: 229–239.

Dziewonski, A.M., Ekström G., Franzen, J.E. and Woodhouse, J.H., 1987b. Global seismicity of 1978: centroid-moment tensor solutions for 512 earthquakes. Phys. Earth Planet. Inter., 46: 316–342.

Dziewonski, A.M., Ekström, G., Franzen, J.E. and Woodhouse, J.H., 1987c. Global seismicity of 1979: centroid-moment tensor solutions for 524 earthquakes. Phys. Earth Planet. Inter., 48: 18–46.

Dziewonski, A.M., Ekström, G., Franzen, J.E. and Woodhouse, J.H., 1988a. Global seismicity of 1980: centroid-moment tensor solutions for 515 earthquakes. Phys. Earth Planet. Inter., 50: 127–154.

Dziewonski, A.M., Ekström, G., Franzen, J.E. and Woodhouse, J.H., 1988b. Global seismicity of 1981: centroid-moment tensor solutions for 542 earthquakes. Phys. Earth Planet. Inter., 50: 155–182.

Dziewonski, A.M., Ekström, G., Woodhouse, J.H. and Zwart, G., 1988c. Centroid-moment tensor solutions for April–June 1987. Phys. Earth Planet. Inter., 50: 215–225.

Ekström, G. and Dziewonski, A.M., 1985. Centroid-moment tensor solutions for 35 earthquakes in western North America (1977–1983). Bull. Seismol. Soc. Am., 75: 23–39.

Ekström, G., Dziewonski, A.M. and Steim, J.M., 1986. Single station CMT; application to the Michoacan, Mexico, earthquake of September 19, 1985. Geophys. Res. Lett., 13: 173–176.

Fujita, K. and Kanamori, H., 1981. Double seismic zones and stresses of intermediate depth earthquakes. Geophys. J.R. Astron. Soc., 66: 131–156.

Giardini, D., 1983. Regional deviation of earthquake source mechanisms from the 'double couple' model. In: H. Kanamori and E. Boschi (Editors), Earthquakes: Observation North-Holland, Amsterdam, Theory and Interpretation, pp. 345–353.

Giardini, D., 1984. Systematic analysis of deep seismicity: 200 centroid-moment tensor solutions for earthquakes between 1977 and 1980. Geophys. J.R. Astron. Soc., 77: 883–914.

Gilbert, F. and Dziewonski, A.M., 1975. An application of normal mode theory to the retrieval of structural parameters and source mechanisms from seismic spectra. Philos. Trans. R. Soc. London, Ser. A, 278: 187–269.

Gill, P.E., Murray, W. and Wright, M.H., 1981. Practical Optimization, Academic Press, London, 401 pp.

Green, II, H.W. and Burnley, P.C., 1989. A new self-organizing mechanism for deep-focus earthquakes. Nature, 341: 733–737.

Green, II, H.W., Young, T.E., Walker, D. and Scholz, C.H., 1990. Anticrack-associated faulting at very high pressure in natural olivine. Nature, 348: 720–722.

Isacks, B. and Molnar, P., 1969. Mantle earthquake mechanisms and the sinking of the lithosphere. Nature, 223: 1121–1124.

Kawakatsu, H., 1986. Double seismic zones: Kinematics, J. Geophys. Res., 91: 4811–4825.

Kawakatsu, H., 1989. Centroid single force inversion of seismic waves generated by landslides. J. Geophys. Res., 94: 12363–12374.

Kawakatsu, H., 1991a. Insignificant isotropic component in the moment tensor of deep earthquakes, Nature, 351: 50–53.

Kawakatsu, H., 1991b. Enigma of earthquakes at ridge–transform-fault plate boundaries—distribution of non-double couple parameter of Harvard CMT solutions. Geophys. Res. Lett., 18: 1103–1106.

Kawakatsu, H., 1992. On the observability of the isotropic component of a moment tensor. In preparation.

Knopoff, L. and Randall, M.J., 1970. The compensated linear-vector dipole: a possible mechanism for deep earthquakes. J. Geophys. Res., 75: 4957–4963.

Kuge, K., 1991. Non double couple components of deep earthquakes. D. Sc. Thesis, University of Tokyo, 111 pp.

Kuge, K. and Kawakatsu, H., 1990. Analysis of a deep "non-double couple" earthquake using very broadband data. Geophys. Res. Lett., 17: 227–230.

Kuge, K. and Kawakatsu, H., 1992. Deep and intermediate-depth non-double couple earthquakes: interpretation of

moment tensor inversions using various passbands of very broadband seismic data. Geophys. J. Int., in press.

Kumazawa, M. and Anderson, O.R., 1969. Elastic moduli, pressure derivatives, and temperature derivatives of single-crystal olivine and single-crystal forsterite. J. Geophys. Res., 74: 5961–5972.

Masters, G. and Gilbert, F., 1983. Attenuation in the earth at low frequencies. Philos. Trans. R. Soc. London, Ser. A. 308: 479–522.

Nábělek, J.L., 1984. Determination of earthquake source parameters from inversion of body waves, Ph.D. Thesis, Massachusetts Institute of Technology, Cambridge, MA, 361 pp.

Okino, K., Ando, M., Kaneshima, S. and Hirahara, K., 1989. The horizontally lying slab, Geophys. Res. Lett., 16: 1059–1062.

Riedesel, M.A. and Jordan, T.H., 1989. Display and assessment of seismic moment tensors. Bull. Seismol. Soc. Am., 79: 85–100.

Satake, K., 1985. Effects of station coverage on moment tensor inversion. Bull. Seismol. Soc. Am., 75: 1657–1667.

Solomon, S.C. and Julian, B.R., 1974. Seismic constraints on ocean-ridge mantle structure: anomalous fault-plane solutions from first motions. Geophys. J.R. Astron. Soc., 38: 265–285.

Vasco, D.W., 1990. Moment-tensor: searching for non-double couple earthquakes. Bull. Seismol. Soc. Am., 80: 354–371.